Non-LTE modelling of cyanoacetylene: evidence for isomer-specific excitation

Cheikh Bop, François Lique, Alexandre Faure, Ernesto Quintas-Sánchez, Richard Dawes

MNRAS **000**, 1–?? (2020) Preprint 24 November 2020 Compiled using MNRAS LATEX style file v3.0

Non-LTE modelling of cyanoacetylene: evidence for isomer-specific excitation

Cheikh T. Bop[1]★, François Lique[1]†, Alexandre Faure[2], Ernesto Quintas-Sánchez[3], and Richard Dawes[3]

[1]*Laboratoire Ondes et Milieux Complexes (LOMC), UMR 6294, Centre National de la Recherche Scientifique (CNRS)-Université du Havre, 25 Rue Philippe Lebon, BP 1123, F-76063 Le Havre, France*

[2]*Université Grenoble Alpes, Centre National de la Recherche Scientifique (CNRS), Institut de Planétologie et d'Astrophysique de Grenoble (IPAG), F-38000 Grenoble, France*

[3]*Department of Chemistry, Missouri University of Science and Technology, Rolla, Missouri 65409, United States*

Accepted XXX. Received YYY; in original form ZZZ

ABSTRACT

Cyanoacetylene molecules are widespread in the interstellar medium (ISM) and several of its isomers have been detected in cold molecular clouds and circumstellar gas. Accurate estimates of the abundance ratio of cyanoacetylene isomers may provide deep insight into their environment. Such knowledge requires rigorous modeling of the emission spectra based on non-Local Thermodynamic Equilibrium (LTE) radiative transfer calculations. To this end, we computed excitation cross sections of HC_2NC and HNC_3 induced by collision with para- and ortho-H_2, using a quantum mechanical close-coupling method. Then, by thermally averaging these data, we derived rate coefficients for the first 31 low-lying rotational levels of each isomer for temperatures up to 80 K. For the para-H_2 collider, the propensity rules are in favor of rotational transitions involving $\Delta j_1 = 2$ for both isomers; while for the ortho-H_2 collider, $\Delta j_1 = 2$ and $\Delta j_1 = 1$ rotational transitions are favored for HC_2NC and HNC_3, respectively. A comparison of rate coefficients for the HC_3N isomers shows differences up to an order of magnitude, especially at low temperatures. Finally, we performed non-LTE radiative transfer calculations to assess the impact of such variations in the analysis of observations. Our simulation suggests that the lack of collisional data specific to each isomer could lead to errors up to a factor of 2–3 in the excitation temperatures. We expect that these data could help in better understanding the cyanoacetylene chemistry and constraining the nitrogen chemistry in the ISM.

Key words: ISM: molecules – molecular data – molecular processes – ISM : abundances

1 INTRODUCTION

The cyanopolyynes, namely $HC_{2n+1}N$ ($n = 1, 2, 3, ...$), are rod-like shaped nitriles which are made up of $2n$ carbon atoms bonded at the ends with a hydrogen atom (H) and a cyanide (CN) group. Since they usually have a low rotational constant and a relatively large dipole moment, which make them ideal barometers and thermometers of their astronomical environments (Cordiner et al. 2011, 2013), they are known as good gas-tracers. For instance, cyanoacetylene (HC_3N), which has a rotational constant of ~ 0.152 cm^{-1} (Creswell et al. 1977) and a dipole moment of ~ 3.7 D (DeLeon & Muenter 1985), is found to be a good tracer for warm and dense regions (Costagliola & Aalto 2010). In addition, HC_3N can also be used to understand the evolution of physical conditions of molecular clouds, as recently done by Al-Edhari et al. (2017). Indeed, these authors used HC_3N and HC_5N emission spectra to unveil a crucial part of the IRAS 16293-2422 history, as they found that the source underwent a moderately rapid collapse and then a very rapid heating of the cold matter to 80 K. Cyanoacetylene is then of particular interest in astrochemistry.

Like most cyanides, cyanoacetylene displays structural isomerism. So far, four stable isomers of HC_3N—namely C_2(H)CN, HNC_3, $HCNC_2$, and HC_2NC—have been detected in laboratory experiments. Among them, only HNC_3 and HC_2NC were observed in the interstellar and circumstellar gas (Kawaguchi et al. 1992a,b; Gensheimer 1997). The abundance ratio of isomers constitutes a useful tool to probe the physical and chemical conditions in the interstellar medium (ISM), as illustrated by Hacar et al. (2020). Therefore, accurately determining the abundance ratios between HC_3N and its isomers may reveal important information about the media in which they are observed.

★ cheikhtidiane.bop@ucad.edu.sn
† francois.lique@univ-lehavre.fr

Very recently, determination of the abundance ratio of the HC_3N isomers has been performed in several sources. In the L1544 prestellar core, Vastel et al. (2018) derived $[HC_3N]/[HC_2NC]$ and $[HC_3N]/[HNC_3]$ abundance ratios of 28 – 73 and 320 – 800, respectively. In L483, Agúndez et al. (2019) derived the $[HC_3N]/[HC_2NC] \simeq 74$ and $[HC_3N]/[HNC_3] \simeq 840$ abundance ratios. Cernicharo et al. (2020) derived, respectively, values of 77 ± 8 and 442 ± 70 for these ratios in TMC-1, and values of 392 ± 22 and 1305 ± 45 in the IRC+10216 circumstellar envelope. All these studies concluded that HC_3N is the most abundant isomer, followed by HC_2NC and HNC_3, respectively. However, the abundance ratio of these isomers varies greatly from one source to another.

Vastel et al. (2018) used an astrochemical model to explain the abundance ratios derived from observations. They considered that the formation of HC_3N isomers is likely to take place through dissociative recombination (DR) of HC_3NH^+:

$$HC_3NH^+ + e^- \rightarrow HC_3N + H \quad (1)$$
$$\rightarrow HC_2NC + H \quad (2)$$
$$\rightarrow HNC_3 + H \quad (3)$$

Based on the branching ratios for the DR of DC_3ND^+ measured by Vigren et al. (2012), they estimated ratios of 22 %, 4 %, and 22 % for the reactions (1), (2), and (3), respectively. HC_3N is also formed through neutral–neutral reactions. This model reproduces fairly well the observed abundances of HC_3N isomers in L1544, although it tends to overestimate the abundances of HC_2NC, and especially HNC_3, with respect to HC_3N. The same conclusion was found by the astrochemical model of Osamura et al. (1999), performed for TMC-1. On one hand, such disagreements between astrochemical models and observations may indicate that different formation mechanisms could be involved. On the other hand, the abundance of HC_3N isomers derived from the observations may also be uncertain because of the lack of available collisional data. Indeed, molecular abundances derivation should be performed using radiative transfer models beyond the Local Thermodynamic Equilibrium (LTE) approximation and therefore, requires the prior study of collisional excitation. Such studies currently exist only for the HC_3N molecule.

The collisional excitation of HC_3N by He and H_2 was first studied by Morris et al. (1976). Few time after, Green & Chapman (1978) determined HC_3N–He rate coefficients using a potential energy surface (PES) obtained from an approximate 'electron gas' model combined with a Monte Carlo quasi-classical trajectory (QCT) method. The first quantum study was performed by Wernli et al. (2007); they investigated the scattering of HC_3N induced by collisions with He and para-$H_2(j_2 = 0)$, j_2 being the H_2 rotational momentum. These calculations were extended to the ortho-$H_2(j_2 = 1)$ collider by Faure et al. (2016).

As the HC_3N isomers were not the object of any collisional excitation studies, rate coefficients for the HC_3N molecule could only be used as a surrogate to model the emission spectra of its isomers (Cernicharo et al. 2020). It was recently shown (Hernández Vera et al. 2017) that isomerism effects can be important in collisional studies, and that rate coefficients can differ significantly for different isomers. Hence, we recently reported the first four dimensional (4D) PESs for the HC_2NC–H_2 and HNC_3–H_2 systems, as well as excitation rate coefficients due to para-$H_2(j_2 = 0)$ [hereafter p-$H_2(j_2 = 0)$] collisions for temperature below 20 K (Bop et al. 2019). These data highlighted different excitation efficiencies for the HC_3N isomers.

In this work, we extend our previous collisional excitation study of the HC_3N isomers to higher temperatures and to the ortho-$H_2(j_2 = 1)$ [hereafter o-$H_2(j_2 = 1)$] collider. Brief descriptions of the PESs and the quantum scattering methodology are presented in section 2. Rotational cross sections and rate coefficients of HC_2NC and HNC_3 induced by collisions with both o-$H_2(j_2 = 1)$ and p-$H_2(j_2 = 0)$ are presented in section 3. In section 4 we study the excitation of the HC_3N isomers in astrophysical media, and concluding remarks are given in section 5.

2 METHODS

2.1 HC_2NC–H_2 and HNC_3–H_2 potential energy surfaces

Using the CCSD(T)-F12b[1] approach (Adler et al. 2007), along with the VTZ-F12[2] basis set (Hill et al. 2010), we derived 4D PESs for the HC_2NC–H_2 and HNC_3–H_2 van der Waals (vdW) systems within the rigid rotor approximation. As we have done in the past for other vdW linear dimers (Wang et al. 2016; Donoghue et al. 2016; Barclay et al. 2018; Desrousseaux et al. 2019; Castro-Juárez et al. 2019; Quintas-Sánchez et al. 2020), the 4D PES analytical representation was constructed using an automated interpolating moving least squares methodology (Dawes et al. 2010; Majumder et al. 2016), implemented in the recently released software-package `AUTOSURF` (Quintas-Sánchez & Dawes 2019). The global estimated root-mean-squared fitting error tolerance was 0.33 cm^{-1} for both PESs, and the total number of symmetry unique points needed to reach that target was 6095 for HC_2NC–H_2 and 4172 for HNC_3–H_2. As usual (Dawes & Quintas-Sánchez 2018), a local fit was expanded about each data point, and the final potential is obtained as the normalized weighted sum of the local fits. The `MOLPRO` electronic structure package (Werner et al. 2012) was used to perform all the *ab initio* calculations used to fit the PESs. These vdW complexes present each two minima; with well-depths of 174.1 cm^{-1} and 178.0 cm^{-1} for HC_2NC–H_2, and 270.8 cm^{-1} and 467.9 cm^{-1} for HNC_3–H_2. More details concerning the computational details, as well as the analytical representation, well-depths and its precise locations for each PESs, can be obtained in Bop et al. (2019).

In order to perform quantum scattering calculations, the angular dependence of the PES was refitted over spherical harmonics. Due to the high-anisotropy, the regularization procedure of Wernli et al. (2007) was employed. The final expansion included 380 angular basis functions and each expansion coefficient was interpolated radially in the range R = 5–30 a_0 with a smooth connection to standard short- and long-range extrapolations. Full details can be found in Bop et al. (2019).

2.2 Scattering calculations

In this work, we focus on the rotational transitions of HC_2NC and HNC_3 induced by collision with H_2 molecules:

$$HC_2NC(j_1) + H_2(j_2) \rightarrow HC_2NC(j_1') + H_2(j_2') \quad (4)$$

$$HNC_3(j_1) + H_2(j_2) \rightarrow HNC_3(j_1') + H_2(j_2') \quad (5)$$

where j_1 and j_2 stand for the rotational angular momenta of the HC_3N isomers and H_2, respectively. Separate calculations were done for p-H_2 (even j_2) and o-H_2 (odd j_2) since ortho-para-H_2

[1] explicitly correlated coupled cluster with single, double and non-iterative triple excitation

[2] polarized valence triple zeta Gaussian basis set which explicitly treats the correlation of electrons

conversion is not allowed during inelastic collisions. The splitting of the HC_2NC and HNC_3 rotational lines due to the nuclear spin of the N atom is not taken into account here as hyperfine transitions of HC_2NC and HNC_3 are currently not resolved in astrophysical media. Hyperfine resolved rate coefficients can be approximately derived from our data, in case they are needed, using the procedure of Faure & Lique (2012) and Lanza & Lique (2014).

Using the 4D HC_2NC–H_2 and HNC_3–H_2 PESs, we derived inelastic cross sections for the 31 first low-lying rotational levels (j_1 = 0–30) of HC_2NC and HNC_3. The energy levels of the HC_2NC, HNC_3 and H_2 molecules were determined using the experimental rotational and centrifugal distortion constants, B_0 and D_0. For HC_2NC and HNC_3, the two employed constants (B_0, D_0) are (0.166 cm^{-1}, 2.091×10^{-8} cm^{-1}) and (0.156 cm^{-1}, 2.063×10^{-8} cm^{-1}), respectively; while for H_2, B_0 = 59.322 cm^{-1} and D_0 = 0.047 cm^{-1} (Huber & Herzberg 1979). The maximum total energy used in the scattering calculations was set to 500 cm^{-1} and 620 cm^{-1} for p- and o-H_2 calculations (The ground o-H_2(j_2 = 1) level is at about 118 cm^{-1} above the p-H_2(j_2 = 0) level). We used the exact close-coupling (CC) quantum mechanical method (Green 1975) as implemented in the `MOLSCAT` computer code (Hutson & Green 1994). The modified log derivative-airy integrator (Alexander & Manolopoulos 1987) was used to solve the coupled equations.

For both of the HC_2NC–H_2 and HNC_3–H_2 collision systems, for both p- and o-H_2 calculations, the close-coupling equations were propagated from from 2 Å, to at least 25 Å. In order to ensure convergence of the state-to-state inelastic cross sections ($\sigma_{j_1 j_2 \rightarrow j_1' j_2'}$), the rotational bases of the HC_2NC, HNC_3 and H_2 molecules were adjusted as a function of the total energy. For instance, at the highest total energy, j_1 of HC_2NC was fixed at 33 and 34 for p-H_2 and o-H_2 collisions, respectively; while j_1 of HNC_3 remained at 34 for collisions with both spin-isomers (p-H_2 and o-H_2). The cross sections obtained with such rotational basis of the cyanopolyynes differ by less than 1% compared to cross sections obtained with rotational basis of the cyanopolyynes containing 41 levels (e.g. increasing j_1 up to 40).

Only the lowest rotation levels of p-H_2 (j_2 = 0) and o-H_2 (j_2 = 1) were included in the calculations. Table 1 shows the impact of the p-H_2 rotational basis on the magnitude of the cross sections as a function of the energy. Two series of test were performed, the first one was for one single total angular momentum (J = 0) and the second test consists of summing the partial cross sections over the first 11 total angular momenta (J = 0 – 10). We found that the convergence increases when summing over the total angular momentum. For example, in the cases of HC_2NC-p-H_2, summing partial cross-sections up to J = 10 leads to average biases less than ~10% for all considered energies whereas the difference could be greater than a factor 2 for J = 0 only. For HNC_3-p-H_2 and HC_2NC-p-H_2, we found that the convergence with respect to the H_2 basis increases with the increase of the energy and is relatively independent to the energy, respectively.

For HC_2NC-p-H_2, the global convergence of the results considering the minimal H_2 basis is good enough, i.e. better than 10% for all the energy grid considered here. The difference can be higher for state-to-state data but remains below 20-30% for all transitions. For HNC_3-p-H_2, because of the larger well depth in the PES, the deviation is greater but less than 20% beyond 100 cm^{-1}. The large bias (> 50%) obtained at 50 cm^{-1} is due the resonances which are significant because of the deep potential well of this collision system.

From this table, we can see that our cross sections are globally converged to better than 15-20%. In the case of the o-H_2 collider, setting $j_2 = 1 - 3$ instead of j_2 = 1 did not affect much the cross sections (less than 10% of deviation) so that the convergence of the o-H_2 basis is estimated to be better than that of the p-H_2 ones.

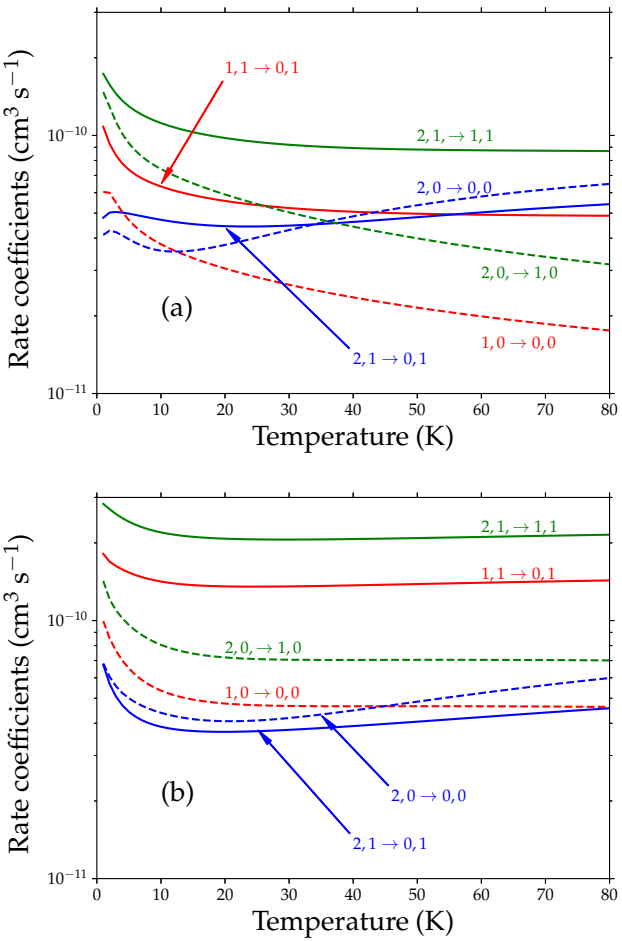

Figure 1. Rotational rate coefficients of HC_2NC [panel (a)] and HNC_3 [panel (b)] induced by collision with p-H_2(j_2 = 0) and o-H_2(j_2 = 1). In both panels, dashed lines stand for the results obtained in the p-H_2 ladder, while solid lines refer to the o-H_2 symmetry. The transitions are labeled as $j_1, j_2 \rightarrow j_1', j_2'$.

We smoothly scanned the total energy range up to 250 cm^{-1} (370 cm^{-1}) for collisions with p-H_2 (o-H_2), with a fine grid step of 0.2 cm^{-1}. Thereafter, we gradually increased this step up to 20 cm^{-1}, which was used in the total energy interval 400–500 cm^{-1} (520–620 cm^{-1}) for the HC_2NC–p-H_2 and HNC_3–p-H_2 (HC_2NC–o-H_2 and HNC_3–o-H_2) collisional systems. Note that the rotational energy at j_1 = 30 for HC_2NC and HNC_3 is 144.14 cm^{-1} and 144.80 cm^{-1}, respectively. Hence, the kinetic energy range used in this work is essentially the same for both isomers.

From the computed cross sections, we derive the corresponding rotational rate coefficients ($k_{j_1 j_2 \rightarrow j_1' j_2'}$) using the Maxwell-Boltzmann thermal average over the kinetic energy:

$$k_{j_1 j_2 \rightarrow j_1' j_2'}(T) = \left(\frac{8}{\pi \mu \beta}\right)^{1/2} \beta^2 \int_0^{\infty} E_c \sigma_{j_1 j_2 \rightarrow j_1' j_2'}(E_c) e^{-\beta E_c} \, dE_c \quad (6)$$

In equation 6, $\beta = (k_B \times T)^{-1}$, with k_B being the Boltzmann con-

Table 1. The effect of the H_2 rotational manifold in the cross-section ($\AA^2$) calculations for selected energies and total angular momenta (J). The values in brackets represent the relative errors (in percent) when restricting j_2 to zero and $< \Delta\sigma >$ stands for the average deviation (in percent) over all inelastic transitions.

HC_2NC–para-H_2													
		E = 50 cm^{-1}				E = 100 cm^{-1}				E = 500 cm^{-1}			
		$J = 0$		$J = 0-10$		$J = 0$		$J = 0-10$		$J = 0$		$J = 0-10$	
j_1	j_1'	$j_2 = 0$	$j_2 = 0-2$	$j_2 = 0$	$j_2 = 0-2$	$j_2 = 0$	$j_2 = 0-2$	$j_2 = 0$	$j_2 = 0-2$	$j_2 = 0$	$j_2 = 0-2$	$j_2 = 0$	$j_2 = 0-2$
1	0	8.03E-3	1.04E-2	6.36E-1	9.10E-1	1.20E-4	2.86E-4	6.61E-3	1.61E-2	2.97E-7	3.01E-5	3.77E-3	2.99E-3
			(22.44)		(30.14)		(58.17)		(58.90)		(90.01)		(26.15)
3	2	6.74E-3	9.77E-3	1.74E+0	1.98E+0	8.38E-6	1.12E-2	8.06E-2	1.15E-1	5.38E-6	6.20E-5	1.17E-2	9.52E-3
			(31.02)		(11.96)		(99.93)		(30.16)		(91.32)		(22.46)
6	4	4.68E-3	5.68E-3	1.27E+1	1.24E+1	1.06E-2	2.55E-4	4.38E+0	4.42E+0	2.50E-4	1.94E-4	3.17E-1	2.78E-1
			(17.61)		(1.86)		(> 100)		(1.04)		(29.11)		(13.96)
8	6	5.09E-3	6.33E-3	1.06E+1	1.04E+1	1.81E-3	3.74E-4	4.29E+0	4.19E+0	1.28E-4	9.32E-5	2.54E-1	2.64E-1
			(19.56)		(1.25)		(> 100)		(2.25)		(37.02)		(3.57)
14	9	9.03E-8	8.31E-8	1.09E+0	9.76E-1	3.21E-4	1.95E-3	4.02E-1	4.15E-1	1.27E-4	5.30E-5	1.40E-1	1.25E-1
			(8.67)		(11.41)		(83.51)		(3.18)		(> 100)		(11.79)
$< \Delta\sigma >$			(29.28)		(6.92)		(> 100)		(9.27)		(> 100)		(10.55)
HNC_3–para-H_2													
2	1	4.30E-3	8.08E-4	2.08E+0	1.17E+0	2.62E-3	3.12E-3	4.80E-1	5.14E-1	9.63E-5	2.96E-4	2.33E-2	3.36E-2
			(> 100)		(77.49)		(15.98)		(6.49)		(67.40)		(30.82)
4	3	1.18E-3	4.42E-3	5.59E+0	4.30E+0	5.55E-4	1.65E-3	9.41E-1	1.27E+0	2.88E-4	7.64E-4	7.52E-2	1.05E-1
			(73.23)		(29.90)		(66.35)		(26.12)		(62.37)		(28.60)
5	7	3.16E-3	9.67E-3	7.50E+0	7.86E+0	4.25E-3	3.96E-4	3.02E+0	3.03E+0	1.66E-4	1.83E-4	2.69E-1	2.19E-1
			(67.31)		(4.63)		(> 100)		(0.57)		(9.62)		(22.87)
7	9	3.15E-4	8.62E-4	7.09E+0	7.36E+0	1.53E-3	9.95E-4	2.36E+0	2.41E+0	9.78E-5	1.89E-4	2.09E-1	2.23E-1
			(63.47)		(3.68)		(53.54)		(2.01)		(48.14)		(6.40)
5	13	8.45E-4	1.11E-3	1.88E+0	2.41E+0	3.18E-4	5.87E-4	1.88E+0	2.04E+0	1.41E-4	1.18E-4	2.06E-1	2.14E-1
			(23.77)		(21.76)		(45.84)		(7.80)		(19.51)		(4.12)
$< \Delta\sigma >$			(> 100)		(61.93)		(>100)		(21.48)		(> 100)		(13.41)

stant and μ being the reduced mass of the collisional system. Since we focus on the 31 low-lying rotational levels of the complexes of interest, the kinetic energy range used in the calculations permitted computation of rate coefficients for temperatures up to 80 K.

3 ROTATIONAL CROSS SECTIONS AND RATE COEFFICIENTS

We display in Fig. 1 the temperature variation of the HC_2NC–H_2 and HNC_3–H_2 rate coefficients. Comparing the plots in the two panels of Fig. 1 reveals that rate coefficients of HNC_3–H_2 are globally larger than those of HC_2NC–H_2. Such behavior can be related to the fact that the minimum of the HNC_3–H_2 interaction potential is $\sim$ 2.5 times deeper than that of HC_2NC–H_2. It is interesting to note that, for both isomers, the temperature variation of the rate coefficients is weak, the rate coefficients being almost constant for temperatures above $\sim$ 20 K. We also observe that the rate coefficients for o-H_2 collisions are larger than those for p-H_2 collisions. The difference is however moderate (within a factor of three), as previously found for HC_3N–H_2 collisions (Faure et al. 2016).

To gain further insight into propensity rules, we plot in Fig. 2 the de-excitation rate coefficients of the HC_3N isomers out of the $j_1 = 10$ level at 50 K. The HC_3N rate coefficients were taken from Faure et al. (2016). For collisions with p-H_2, for both isomers, one can see that the propensity in favor of even Δj_1 transitions observed in our previous work (Bop et al. 2019) persists at higher temperatures. In contrast, for collisions with o-H_2, the propensity rules are different for the two isomers. A propensity rule in favor of even Δj_1 transitions is found for HC_2NC (however, less marked than for p-H_2 collisions) while for HNC_3, the magnitude of rate coefficients typically follows an energy-gap law, (*i.e.*, $\Delta j_1 = 1 > \Delta j_1 = 2 > \Delta j_1 = 3$ ...). The change of propensity rules with respect to the rotational states of H_2 in the case of HNC_3–H_2 collisions, was also found for the HC_3N–H_2 and HCN–H_2 collisional systems (Faure et al. 2016; Hernández Vera et al. 2017). Such behavior originates from the quadrupole moment of $H_2(j_2 > 0)$ which modifies the interaction with the target. Indeed, the dipole-quadrupole interaction governs the long-range interactions but vanishes for $H_2(j_2 = 0)$. The difference between o- and p-H_2 is marked in the case of HNC_3 since HNC_3 exhibits a strong permanent dipole moment of 5.665 D (Botschwina et al. 1992). Such inversion of the propensity rules is not seen for HC_2NC because of the weaker dipole moment (2.93 D), (Krüger et al. 1991).

In order to check the validity of using the rate coefficients of one isomer to derive the abundance of the other isomers, we depict in Fig. 3 the rate coefficients of HC_2NC and HNC_3 as a function of those of HC_3N and the rate coefficients of HNC_3 as a function of those of HC_2NC. For each isomer, the relative deviation to others is less than a factor of 3 when considering the o-H_2 collider. The deviation is even less than a factor of 1.5–2 when considering only the dominant rate coefficients ($k(T) \geq 10^{-11}$ cm^{3}s^{-1}).

On the other hand, larger differences exist between the excitation of the different isomers induced by collisions with p-H_2. Indeed, the difference can be up to an order of magnitude for the weaker rate coefficients and up to a factor 3 for the dominant ones, regardless of temperature. It is interesting to note that the rate coefficients of HC_2NC and HNC_3 globally outweigh those of HC_3N whereas a slight dominance of HNC_3 with respect to HC_2NC is found. The stronger magnitude of the HNC_3–H_2 rate coefficients can be related to the larger well-depth in the interaction potential compared to the two other isomers since all isomers exhibit a similar rotational structure.

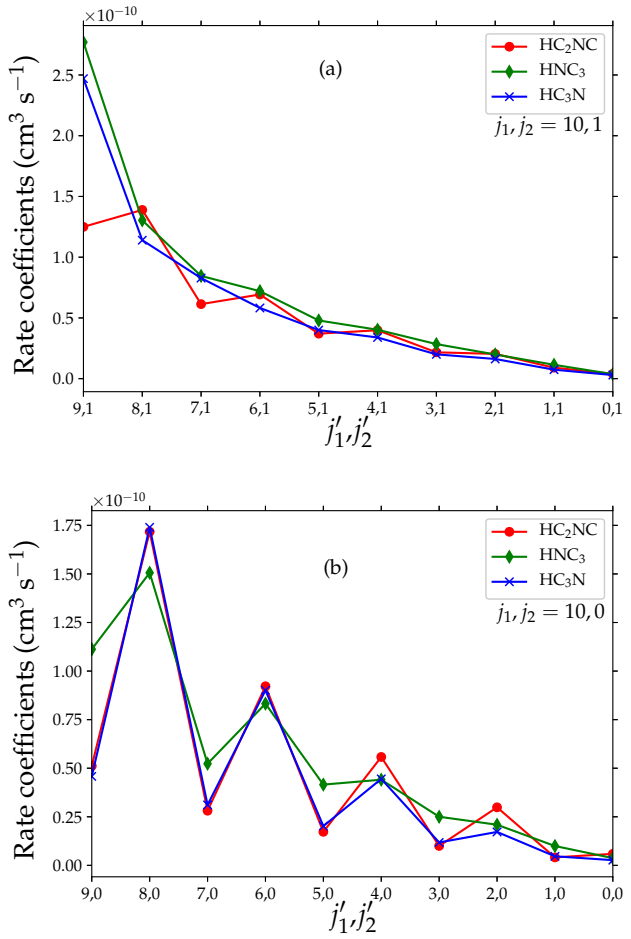

Figure 2. Downward rate coefficients of HC_2NC, HNC_3 and HC_3N (Faure et al. 2016) induced by collision with o-H_2 [panel (a)] and p-H_2 [panel (b)] at T = 50 K. The transitions are labeled as $10, 1 \rightarrow j'_1, 1$ and $10, 0 \rightarrow j'_1, 0$ in panels (a) and (b), respectively.

4 THE EXCITATION OF HC_3N, HC_2NC, AND HNC_3 IN ASTROPHYSICAL MEDIA

The comparison of rate coefficients made in the above paragraph showed that HC_3N and its isomers have different excitation behaviours when they collide with molecular hydrogen. It is then of significant interest to simulate the impact of using the appropriate collisional data when deriving the abundance of the HC_3N isomers in astrophysical media.

Non-LTE radiative transfer calculations were performed with the `RADEX` code (Van der Tak et al. 2007), using the escape probability approximation. Our collisional data were combined with spectroscopic data from the Jet Propulsion Laboratory (JPL) catalog, as downloaded from the Cologne Database for Molecular Spectroscopy (CDMS) portal (Müller et al. 2005) [3]. In practice, we calculated the excitation and brightness temperatures (T_{ex} and T_B, respectively) for the $j_1 = 5 \rightarrow 4$, $8 \rightarrow 7$ and $11 \rightarrow 10$ emission lines, that are frequently observed in the interstellar and circumstellar gas (Vastel et al. 2018; Agúndez et al. 2019; Cernicharo et al. 2020). In our simulation, the cosmic microwave background used as background radiation field was set to 2.73 K and the line width Δv to 1 km s^{-1}. The kinetic temperature was fixed at 10 K to simulate the physical conditions of cold molecular clouds such as TMC-1 or L1544, and at 50 K to reach out the temperature of the outer layers of circumstellar envelopes such as IRC+10216. Furthermore, we chose, for the ortho-to-para ratio of H_2, values of 0 (only p-H_2; model 1); and 3, corresponding to the high temperature limit (model 2). However, any o- and p-H_2 proportion can be used in models since we provided state-to-state rate coefficients for both o- and p-H_2 colliders. In practice, the total density of molecular hydrogen $n(H_2)$ was spanned from 10^2 to 10^8 cm^{-3} and the column densities of HC_3N, HC_2NC, and HNC_3 was fixed at $N = 10^{12}$ cm^{-2}. This value is close to the HC_2NC and HNC_3 column density derived in cold molecular clouds (Vastel et al. 2018).[4] Figs. 4, 5, and 6 show the excitation temperature obtained in our simulations as a function of $n(H_2)$.

First, we note a supra-thermal excitation for the $j_1 = 5 \rightarrow 4$ line at 50 K for densities in the 10^4–10^5 cm^{-3} range. Indeed, the excitation temperature (T_{ex}) is larger than the kinetic temperature (T). Then, as expected, for all isomers the excitation temperature varies from $\sim$ 2.73 K to the kinetic temperature (10 K or 50 K). At low H_2 density, the medium is dilute and the excitation temperature is reduced to the cosmic background temperature ($T_{ex} \approx T_{\rm CMB}$ = 2.73 K) while at high H_2 density, T_{ex} tends asymptotically to the adopted kinetic temperature [T = 10 K for panels (a), (b), and (c) and T = 50 K for panels (d), (e), and (f)]. An agreement between the T_{ex} and the kinetic temperature indicates that LTE conditions are fulfilled. According to our calculations, this is true when the H_2 density exceeds $5{\times}10^4$ to 10^6 cm^{-3} depending on the isomers, the o-to-p-H_2 ratios, the emission lines, and the kinetic temperatures. The density at which $T_{ex} = T$ is called the LTE density below. Because of the weak temperature dependence of the rate coefficients, the LTE densities are not significantly influenced by the kinetic temperature. The o-to-p-H_2 ratio also slightly impact the LTE densities because of the moderate difference between o- and p-H_2 rate coefficients. At the opposite, because of the significant variation of the Einstein coefficients with the increasing rotational state, the LTE density changes by up to an order of magnitude when changing from $j_1 = 5 \rightarrow 4$ to $j_1 = 11 \rightarrow 10$. For all isomers, the LTE density is found to be generally larger than the typical densities in both cold molecular clouds and circumstellar envelopes indicating clearly that non-LTE modeling of the emission spectra is mandatory.

We then focus in the intermediate region where radiative and collisional processes are in competition. The corresponding density is called the critical density. The comparison of the T_{ex} of the different isomers reveals that the excitation conditions of HC_3N, HC_2NC and HNC_3 are different for all lines. In particular, we found that $T_{ex}(HC_2NC) > T_{ex}(HC_3N) > T_{ex}(HNC_3)$] and the differences for the T_{ex} can be up to a factor 2–3. This clearly demonstrates that the excitation conditions of the different isomers are quite different and that it is very risky to assume similar T_{ex} for all isomers.

In Table 2, we show the $j_1 = 8 \rightarrow 7$ brightness temperature ratios of the three HC_3N isomers ($T_B[HC_2NC]/T_B[HC_3N]$, $T_B[HNC_3]/T_B[HC_3N]$, and $T_B[HNC_3]/T_B[HC_2NC]$) for two H_2 density and two temperatures.

At high H_2 density ($\sim 10^8$ cm^{-3}), when LTE conditions are fulfilled, the brightness temperature ratios are not equal to unity due

[3] https://cdms.astro.uni-koeln.de/cdms/portal/

[4] An increase of the column density by one or two orders of magnitude does not change the excitation temperature T_{ex}, since the opacity is still low ($\tau << 1$).

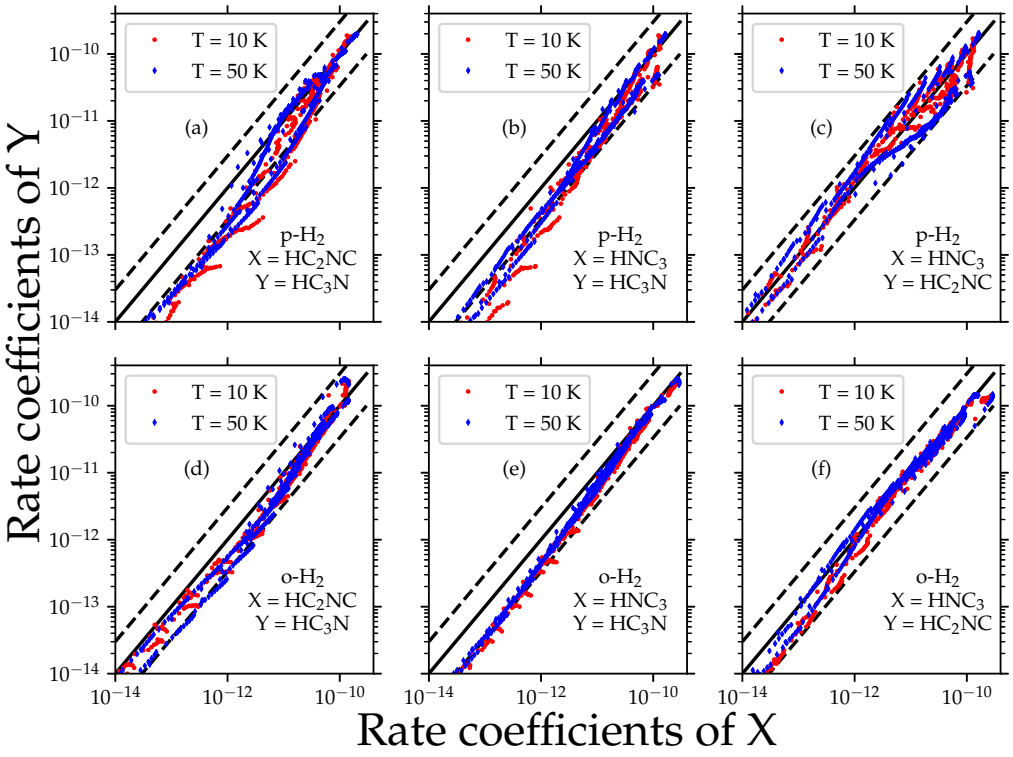

Figure 3. Comparison of rate coefficients of HC_2NC [panels (a) and (d)] and HNC_3 [panels (b) and (e)] to those of HC_3N as well as of HC_2NC to those of HNC_3 [panels (c) and (f)], at T = 10 K and 50 K. The collisions treated in the p-H_2 [o-H_2] ladder are represented in the panels (a), (b) and (c) [(d), (e), and (f)]. In all panels, the diagonal lines are distant from each other by a factor of three and the solid one stands for y = x.

Table 2. Comparison of the brightness temperature ratios and the ratios of the square of the electric dipole moment. The brightness temperatures are calculated at 10 and 50 K. For each line, the first entries and the second entries (values in brackets) were obtained at $n = 10^8$ cm^{-3} and $n = 3 \times 10^4$ cm^{-3}, respectively.

	ratios of T_B		ratios of μ^2
	T = 10 K	T = 50 K	
HC_2NC/HC_3N	0.645	0.721	$0.620^{a,c}$
	(0.725)	(0.686)	
HNC_3/HC_3N	2.299	2.436	$2.319^{b,c}$
	(1.578)	(2.042)	
HNC_3/HC_2NC	3.565	3.377	$3.738^{b,a}$
	(2.177)	(2.976)	

[a] dipole moment of HC_2NC (Krüger et al. 1991)
[b] dipole moment of HNC_3 (Botschwina et al. 1992)
[c] dipole moment of HC_3N (DeLeon & Muenter 1985)

to the difference between the dipole moments of the HC_3N isomers. Indeed, the Einstein coefficients associated to the radiative transitions are proportional to the square of the electric dipole moment (μ^2). We compare in Table 2 the T_B ratios obtained at $n = 10^8$ cm^{-3} to the squared ratios of the dipole moments. For both kinetic temperatures, the agreement is very good, the minor deviations coming from the different frequencies of the cyanopolyynes isomers. In Table 2, we also provide the T_B ratios at $n = 3 \times 10^4$ cm^{-3}, the typical H_2 density in molecular clouds. As one can see, the deviation compared to the squared ratios of the dipole moments is large (up to a factor 2) demonstrating again the importance of non-LTE effects.

Finally, weak maser emissions have been observed for the $j_1 = 1 \rightarrow 0$ (Hunt et al. 1999) and $j_1 = 4 \rightarrow 3$ lines (Ellingsen et al. 2017) of HC_3N. It is then of interest to see if such maser action is predicted for HC_3N isomers. We calculated the excitation temperatures for the $j_1 = 1 \rightarrow 0$ and $4 \rightarrow 3$ line at different temperatures. Below 40 K, no population inversion is predicted for the $4 \rightarrow 3$ line, whereas population inversion occurs even at 10 K for the $1 \rightarrow 0$ line. In Fig. 7, we computed the logarithm of the excitation temperature (see caption) for the $j_1 = 4 \rightarrow 3$ assuming a thermal o- to p-H_2 ratio of ~ 0.3. As can be seen in the figure, population inversion is present for all isomers, depending on the H_2 density. The inversion occurs at larger H_2 densities for HNC_3 than for HC_3N and HC_2NC because of stronger Einstein coefficients. Hence (weak) maser emissions may help to estimate the H_2 density. It is also interesting to note that recent abundance ratio determinations (Cernicharo et al. 2020) were based on the $j_1 = 4 \rightarrow 3$ emission line so that the analysis of such emission spectra in the absence of collisional isomer-specific rate coefficients might be quite uncertain.

5 CONCLUSION

State-to-state excitation cross-sections of HC_2NC and HNC_3 induced by collision with p-H_2 and o-H_2 have been calculated using a close-coupling method. These results were then thermally averaged using a Maxwell-Boltzmann velocity distribution to determine (de)excitation rate coefficients involving the first 31 low-lying rotational levels of both HC_3N isomers for temperatures up to 80 K.

The computed data exhibit some interesting propensity rules. Transitions involving even Δj_1 values are favored for both HC_2NC

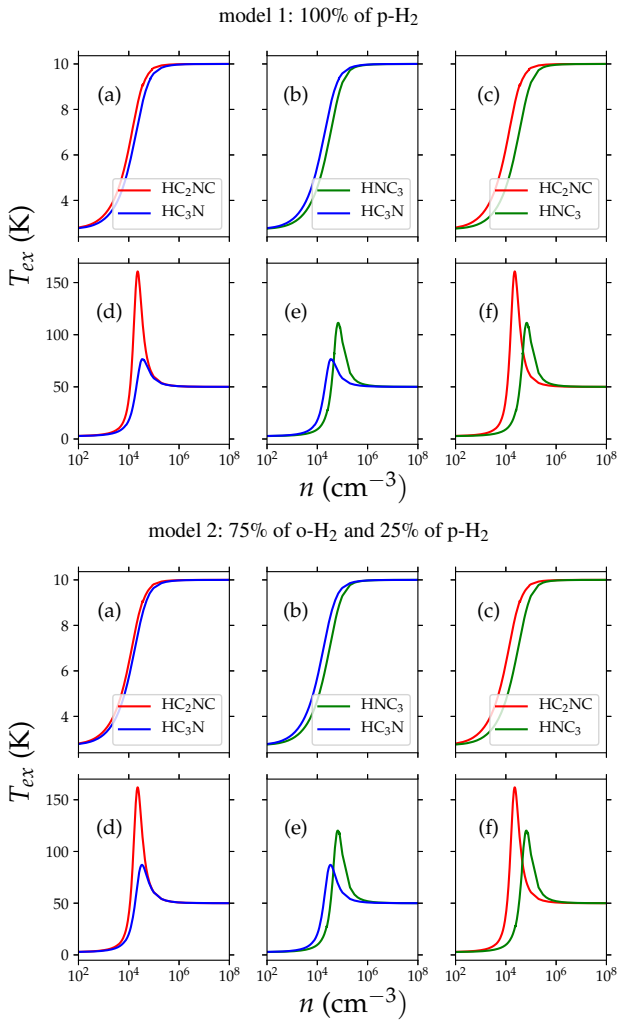

Figure 4. Excitation temperature for the $j_1 = 5 \rightarrow 4$ line of HC_3N, HC_2NC and HNC_3 calculated for temperatures $T = 10$ K [panels (a), (b), and (c)] and $T = 50$ K [panels (d), (e), and (f)] and a fixed column density of 10^{12} cm^{-2} for all isomers. For model 1, only p-H_2 is considered, while in model 2 o- and p-H_2 are in the 3:1 proportion.

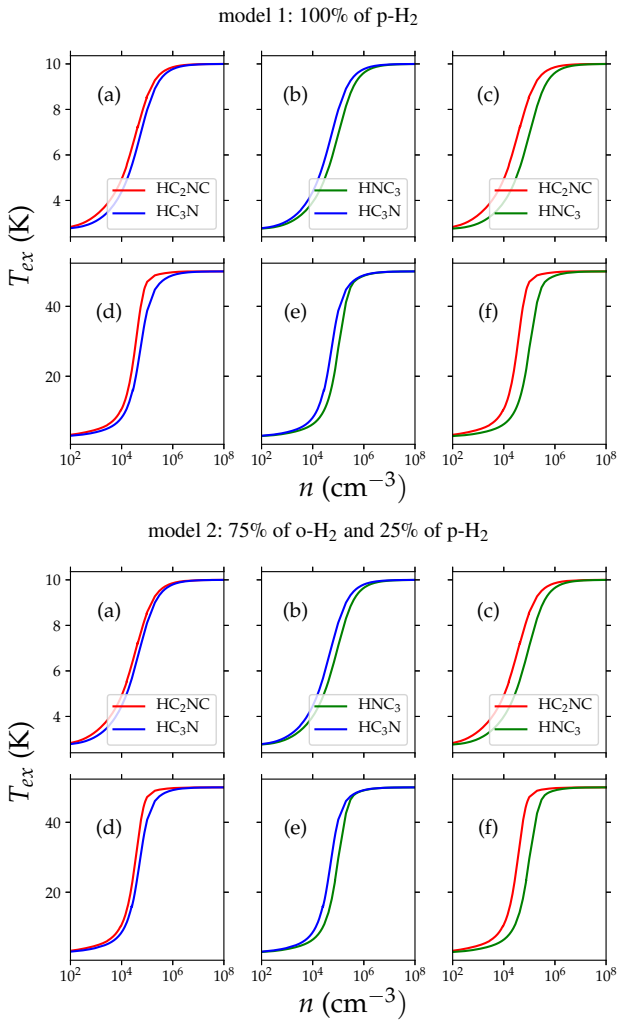

Figure 5. Same as Fig. 4 but for the $j_1 = 8 \rightarrow 7$ line.

and HNC_3 colliding with p-H_2; while for collisions with o-H_2, the propensity is found in favor of $\Delta j_1 = 2$ and $\Delta j_1 = 1$ transitions for HC_2NC and HNC_3 targets, respectively. We found that the HC_2NC and HNC_3 data globally agree within a factor of 3 with those computed for HC_3N by Faure et al. (2016), despite larger differences between some state-to-state transitions. Globally, the HNC_3–H_2 are found to be larger than those of the other isomers.

We also performed radiative transfer calculations for the three cyanopolyynes isomers using the `RADEX` code. The comparison of excitation temperatures showed that the excitation of the three isomers is different and put in evidence the need for specific analysis for the three isomers. In particular, we found that the excitation temperatures of HNC_3 are stronger than that of the other two and clearly demonstrates that special care should be taken when deriving its abundance from the observational spectra. We anticipate that the abundance of HNC_3 derived from the observation may be reduced by the use of an accurate non-LTE model, leading to an even stronger disagreement with astrochemical models.

Numerous studies on excitation of interstellar isomers such as HCN/HNC (Sarrasin et al. 2010; Hernández Vera et al. 2017), AlCN/AlNC (Hernández Vera et al. 2013), MgCN/MgNC (Hernández Vera et al. 2013), SiCN/SiNC (Hernández Vera et al. 2015) and HCO^+/HOC^+ (Santander et al. 2019) have been reported over the last decades. In all these studies, differences ranging from few tenths of a percent up to one order of magnitude were found. It is then clear that ideally, excitation conditions of all isomers should be studied individually, and we strongly recommend to compute specific rate coefficients of the astrophysical isomers in order to accurately determine their abundance ratios. This will lead to better insights about their mechanism of formation in the ISM and will put more robust constraints on astrochemical models. Among the interstellar isomers, the cyanopolyynes are of great interest, and a possible target for future excitation studies could be the HC_4NC molecule, an isomer of the ubiquitous HC_5N that was recently detected in TMC-1 (Xue et al. 2020).

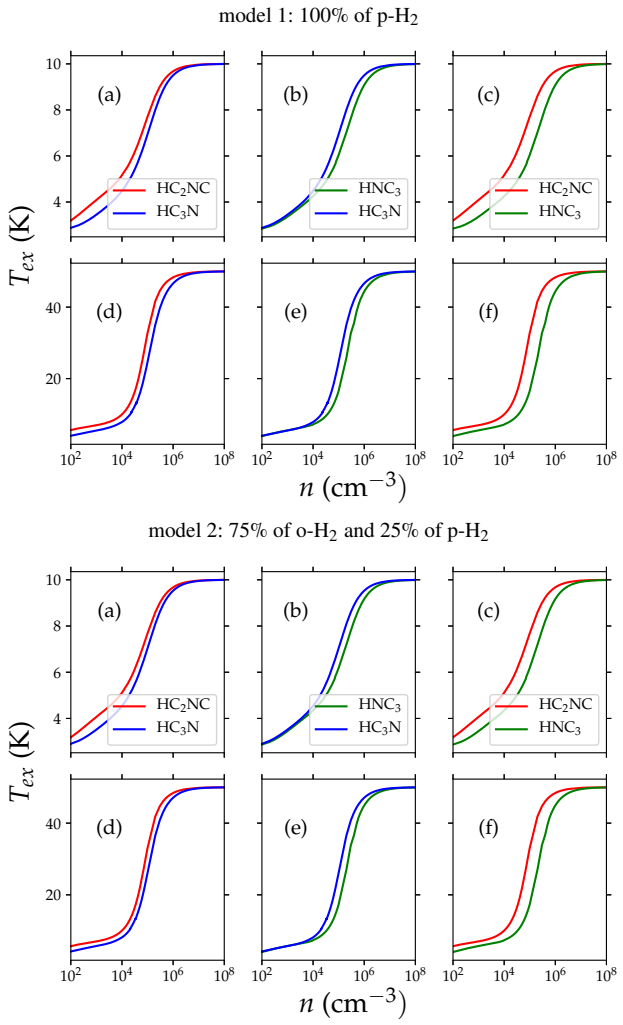

Figure 6. Same as Fig. 4 but for the $j_1 = 11 \rightarrow 10$ line.

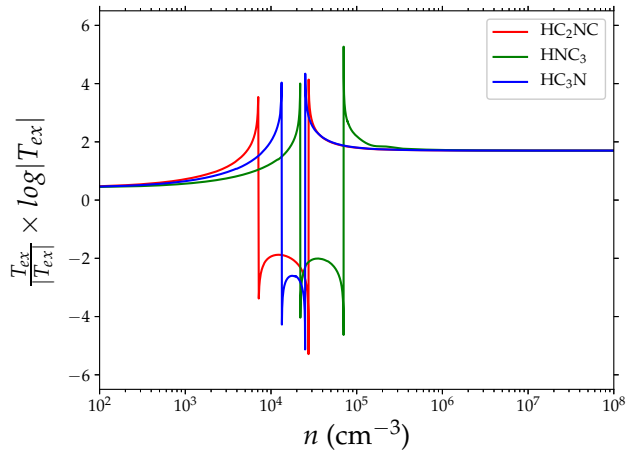

Figure 7. Excitation temperature for the $j_1 = 4 \rightarrow 3$ line of HC_3N, HC_2NC and HNC_3 calculated for a temperature of 50 K and a fixed column density of 10^{12} cm^{-2}, for all isomers.

ACKNOWLEDGMENTS

The authors acknowledge the Programme National "Physique et Chimie du Milieu Interstellaire" (PCMI) of Centre National de la Recherche Scientifique (CNRS)/Institut National des Sciences de l'Univers (INSU) with Institut de Chimie (INC)/Institut de Physique (INP) co-funded by Commissariat a l'Energie Atomique (CEA) and Centre National d'Etudes Spatiales (CNES). FL acknowledges financial support from the Institut Universitaire de France and the French National Research Agency (ANR) through a grant to the Anion Cos Chem Project (ANR-14-CE33-0013). R.D. and E.Q-S. are supported by the US Department of Energy Office of Science, Office of Basic Energy Sciences (Award DE-SC0019740). This work was performed using HPC resources from GENCI-CINES (Grant No. A0070411036), as well as the GRICAD infrastructure (https://gricad.univ-grenoble-alpes.fr), which is supported by Grenoble research communities.

DATA AVAILABILITY

The data underlying this article are available in the article and in its online supplementary material.

REFERENCES

Adler T. B., Knizia G., Werner H.-J., 2007, The Journal of Chemical Physics, 127, 221106
Agúndez M., Marcelino N., Cernicharo J., Roueff E., Tafalla M., 2019, A&A, 625, A147
Al-Edhari A. J., et al., 2017, Astronomy & Astrophysics, 597, A40
Alexander M. H., Manolopoulos D. E., 1987, The Journal of chemical physics, 86, 2044
Barclay A., McKellar A., Moazzen-Ahmadi N., Dawes R., Wang X.-G., Carrington T., 2018, Phys. Chem. Chem. Phys., 20, 14431
Bop C. T., Batista-Romero F. A., Faure A., Quintas-Sánchez E., Dawes R., Lique F., 2019, ACS Earth and Space Chemistry, 3, 1151
Botschwina P., Horn M., Seeger S., Flügge J., 1992, Chemical physics letters, 195, 427
Castro-Juárez E., Wang X.-G., Carrington Jr T., Quintas-Sánchez E., Dawes R., 2019, J. Chem. Phys., 151, 084307
Cernicharo J., Marcelino N., Agundez M., Bermudez C., Cabezas C., Tercero B., Pardo J. R., 2020, arXiv e-prints, p. arXiv:2009.07686
Cordiner M. A., Charnley S. B., Wirström E. S., Smith R. G., 2011, The Astrophysical Journal, 744, 131
Cordiner M., Buckle J., Wirström E., Olofsson A., Charnley S., 2013, The Astrophysical Journal, 770, 48
Costagliola F., Aalto S., 2010, Astronomy & Astrophysics, 515, A71
Creswell R., Winnewisser G., Gerry M., 1977, Journal of Molecular Spectroscopy, 65, 420
Dawes R., Quintas-Sánchez E., 2018, in , Reviews in Computational Chemistry vol. 31. Wiley, Chapt. 5, pp 199–264, doi:10.1002/9781119518068.ch5, https://onlinelibrary.wiley.com/doi/abs/10.1002/9781119518068.ch5
Dawes R., Wang X.-G., Jasper A. W., Carrington Jr T., 2010, J. Chem. Phys., 133, 134304
DeLeon R. L., Muenter J., 1985, The Journal of chemical physics, 82, 1702
Desrousseaux B., Quintas-Sánchez E., Dawes R., Lique F., 2019, J. Phys. Chem. A, 123, 9637
Donoghue G., Wang X.-G., Dawes R., Carrington Jr T., 2016, J. Mol. Spectrosc., 330, 170
Ellingsen S. P., Chen X., Breen S. L., hua Qiao H., 2017, The Astrophysical Journal, 841, L14
Faure A., Lique F., 2012, Monthly Notices of the Royal Astronomical Society, 425, 740

Faure A., Lique F., Wiesenfeld L., 2016, Monthly Notices of the Royal Astronomical Society, 460, 2103
Gensheimer P. D., 1997, Ap&SS, 251, 199
Green S., 1975, The Journal of Chemical Physics, 62, 2271
Green S., Chapman S., 1978, The Astrophysical Journal Supplement Series, 37, 169
Hacar A., Bosman A. D., van Dishoeck E. F., 2020, A&A, 635, A4
Hernández Vera M., Lique F., Dumouchel F., Kłos J., Rubayo Soneira J., Senent M. L., 2013, MNRAS, 432, 468
Hernández Vera M., Lique F., Kłos J., Dumouchel F., Rubayo Soneira J., 2015, MNRAS, 451, 1199
Hernández Vera M., Lique F., Dumouchel F., Hily-Blant P., Faure A., 2017, Monthly Notices of the Royal Astronomical Society, 468, 1084
Hill J. G., Mazumder S., Peterson K. A., 2010, The Journal of chemical physics, 132, 054108
Huber K., Herzberg G., 1979, Van Rostrand-Reinhold, New York
Hunt M. R., Whiteoak J. B., Cragg D. M., White G. L., Jones P. A., 1999, MNRAS, 302, 1
Hutson J., Green S., 1994, Swindon, UK
Kawaguchi K., Ohishi M., Ishikawa S.-I., Kaifu N., 1992a, The Astrophysical Journal, 386, L51
Kawaguchi K., et al., 1992b, The Astrophysical Journal, 396, L49
Krüger M., Dreizler H., Preugschat D., Lentz D., 1991, Angewandte Chemie International Edition in English, 30, 1644
Lanza M., Lique F., 2014, The Journal of chemical physics, 141, 164321
Majumder M., Ndengue S. A., Dawes R., 2016, Molecular Physics, 114, 1
Morris M., Turner B., Palmer P., Zuckerman B., 1976, The Astrophysical Journal, 205, 82
Müller H. S., Schlöder F., Stutzki J., Winnewisser G., 2005, Journal of Molecular Structure, 742, 215
Osamura Y., Fukuzawa K., Terzieva R., Herbst E., 1999, The Astrophysical Journal, 519, 697
Quintas-Sánchez E., Dawes R., Wang X.-G., Carrington T., 2020, Physical Chemistry Chemical Physics
Quintas-Sánchez E., Dawes R., 2019, Journal of Chemical Information and Modeling, 59, 262
Santander C., Urzua-Leiva R., Stoecklin T., Denis-Alpizar O., 2019, The Journal of Physical Chemistry A, 123, 10990
Sarrasin E., Abdallah D. B., Wernli M., Faure A., Cernicharo J., Lique F., 2010, Monthly Notices of the Royal Astronomical Society, 404, 518
Van der Tak F., Black J. H., Schöier F., Jansen D., van Dishoeck E. F., 2007, Astronomy & Astrophysics, 468, 627
Vastel C., Kawaguchi K., Quénard D., Ohishi M., Lefloch B., Bachiller R., Müller H., 2018, Monthly Notices of the Royal Astronomical Society: Letters, 474, L76
Vigren E., et al., 2012, Planetary and Space Science, 60, 102
Wang X.-G., Carrington Jr T., Dawes R., 2016, J. Mol. Spectrosc., 330, 179
Werner H.-J., Knowles P. J., Knizia G., Manby F. R., Schütz M., 2012, Wiley Interdisciplinary Reviews: Computational Molecular Science, 2, 242
Wernli M., Wiesenfeld L., Faure A., Valiron P., 2007, Astronomy & Astrophysics, 464, 1147
Xue C., et al., 2020, The Astrophysical Journal, 900, L9